ACS OMEGA

http://pubs.acs.org/journal/acsodf

Article

Hidden Complexity in the Mechanism of the Autoreduction of Myoglobin Compound II

Kamisha R. Hill, Breanna G. Bailey, Meghan B. Mouton, and Heather R. Williamson*

Cite This: *ACS Omega* 2022, 7, 22906−22914

Read Online

ACCESS | Metrics & More | Article Recommendations | Supporting Information

ABSTRACT: The non-native oxidation of horse heart myoglobin with hydrogen peroxide produces compound II which autoreduces by utilizing an internal oxidation site. Here, we utilize full UV−visible time-dependent kinetics with global kinetic singular value decomposition analysis to explore the mechanism and uncover more detail about the high-valent heme spectral features. By varying the hydrogen peroxide and myoglobin concentration, we were able to uncover more detailed spectra of myoglobin compound II and the autoreduction rate under several different pH conditions. The compound II spectra demonstrate pH-dependent features with an inflection point around pH 5.7 ± 0.1. The rate of autoreduction of compound II, k_2, increases with lower pH with a half-power proton dependence and no indication of a pK_a > 3.9 ± 0.2, indicating that the autoreduction is still dependent on the protonation of the ferryl oxo species. The k_2 also demonstrates both hydrogen peroxide and myoglobin dependency. At myoglobin concentrations greater than 6.6 μM, the k_2 is myoglobin-independent, but for lower concentrations, a pH-sensitive concentration dependence is seen.

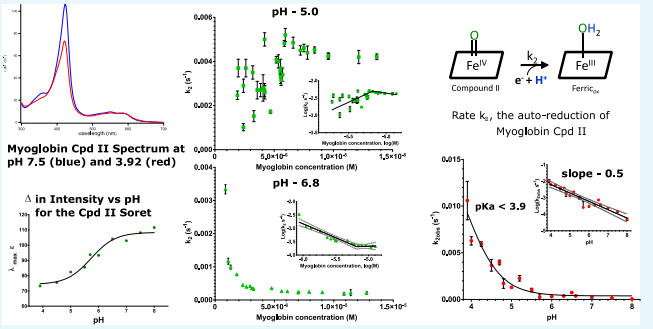

1. INTRODUCTION

Many studies have investigated the formation and reactivity of high-valent myoglobin (Mb) species using various bioanalytical techniques[1−6] in order to resolve the dispute over the nature of the ferryl group in Mb compound II (Cpd II). Several studies using crystallography, magnetic circular dichroism (MCD), and resonance Raman (RR) spectroscopy suggested the existence of a low-pH form of Cpd II, which these authors propose as a protonated ferryl hydroxide (Fe^{IV}−OH) with a pK_a of the Mb ferryl oxo as ∼ 4.5.[2−4] However, other studies using X-ray absorption spectroscopy, Mossbauer, and additional RR spectroscopic methods indicated no protonation of the ferryl oxo in pH conditions as low as 3.9,[4,5] and attribute any different low-pH forms of Fe^{IV}=O to some type of hydrogen bonding to the ferryl oxo.[5] One of the most common methods to generate high-valent species is to react ferric Mb with hydrogen peroxide. The bimolecular reaction generates compound I (Cpd I), which is a ferryl (Fe^{IV}=O) heme species with a radical cation on the heme porphyrin ring. Cpd I rapidly reduces to a long-lived Cpd II via an internal charge transfer between the protein backbone and the heme cofactor.[6] An alternate peroxide reaction pathway was also observed[6] involving homolytic peroxide cleavage, which directly forms Cpd II and rapidly generates a protein radical via a hydroxyl radical. In the absence of an exogenous substrate, the resulting Mb Cpd II then autoreduces to a ferric Mb species, typically with oxidative damage in the peptide or porphyrin.[7−11]

In order to study this autoreduction of Mb Cpd II, many different conditions have been used to both initiate and observe the autoreduction reaction. Many spectroscopic studies, such as Mossbauer, RR spectroscopy, and XAFS,[4,5] use relatively high Mb concentrations, in the millimolar range in order to observe the specific spectroscopic signal being probed with sufficient sensitivity. Visible spectroscopies examining the Q bands, such as time-resolved UV−visible spectroscopy[2] and MCD,[3] often use high micromolar levels, while other studies[1] used lower micromolar levels when exploring the full spectrum to avoid saturating the intense Soret bands. In order to isolate Cpd II, each experiment can use anywhere from low micromolar concentrations of hydrogen peroxide in single-turnover conditions to high millimolar concentrations for reactions with excess levels of peroxide. All of these studies have assumed that neither the concentration of Mb nor that of hydrogen peroxide affects the kinetics of the Cpd II autoreduction as this reaction is only considered a single electron transfer step that is rate-limited by a single proton transfer to the ferryl oxo.[4,5,12−14] Under this

Received: May 5, 2022
Accepted: June 6, 2022
Published: June 16, 2022

assumption, the electron source would not affect the rate of Cpd II autoreduction regardless of the location, or site; however, the proton source should do so.

Neither the proton nor electron transfer was assumed to be dependent on the concentration of the initial oxidant (hydrogen peroxide) in these studies, where the peroxide should be either consumed[2] or neutralized[5,12,13,15,16] before the point Mb Cpd II decays. However, there is evidence that the source of the electron is actually affected both by the presence of multiple Mb proteins and the initial hydrogen peroxide oxidant. The source of the protein oxidation for the autoreduction of Mb Cpd II has been narrowed to the combination of three surface Tyr,[15−19] a surface Trp,[16,17] (both potentially making Mb crosslinked dimers), and a His[15] (which along with a specific Tyr can make a crosslink with the heme moiety[17,20]). In several of these cases, the hydrogen peroxide concentration has been demonstrated to have certain effects on both the initial protein radical from Cpd II formation and the final ferric Mb oxidation product.[20−23] The dimer formation has clear evidence of being dependent on protein concentration.[16]

In order to uncover more information about Mb Cpd II autoreduction and how it is coupled to the protein's auto-oxidation, we present in this study an in-depth time-resolved UV−visible spectroscopy encompassing the full spectrum of the heme group across a range of stable pH values, Mb concentrations, and hydrogen peroxide concentrations. These conditions allow us to analyze relevant spectral features across the visible spectral range of the ferric, ferryl, and oxidatively damaged horse heart Mb at various pHs in order to uncover additional features of the mechanism. By using saturated peroxide conditions and global analysis, we were able to obtain Cpd II spectra at low pH and to resolve the Cpd II autoreduction rate for pH as low as 3.92, which is the lowest pH maintaining a stable protein fold. By having a large pH variation of stable protein, we were able to isolate the exact transition pH for acidic ("acid") and alkaline ("basic") forms of horse heart Mb Cpd II.[3,24] This transition is found to be 5.7 ± 0.1, which corresponds closely to the pK_a of the distal histidine (His64).[12] The pH dependency of the autoreduction rate using our conditions reflects neither an inflection point nor a proton-independent region. Therefore, we consider the rate-limiting protonation event in the Cpd II autoreduction likely to be protonation of the ferryl oxo occurring at a pK_a < 3.9 ± 0.2, as postulated previously by Green and co-workers.[4,5] Unlike earlier studies, we observe a half-order proton dependency for the autoreduction rate, which suggests a more complex mechanism for this step. We also found the rate for the autoreduction step to be dependent not only on pH but also on both Mb and hydrogen peroxide concentrations under certain reaction conditions. While at Mb concentrations above 6.6 μM, we observe the autoreduction rate to be effectively independent of the Mb concentration, at Mb concentrations below 6.6 μM, the rate varies, demonstrating a roughly linear dependency at pH 5.0 and an inverse concentration dependency on pH 6.8.

2. MATERIALS AND METHODS

2.1. Materials. Horse heart Mb and catalase were purchased from Sigma-Aldrich. The Mb was oxidized to iron (III) by ferricyanide, desalted with a PD10 column, and stored in 50 mM sodium acetate buffer at pH 5.0. Concentrations of stocks were determined through absorbance with a reference of $A_{409\ nm}$= 171 mM^{-1} cm^{-1}. Hydrogen peroxide 30% was purchased from Thermo Fisher Scientific.

2.2. Time-Resolved Spectroscopy. The peroxide saturating condition reaction data were collected using a Cary60 UV−vis spectrophotometer and an OLIS HP8452A diode array spectrophotometer, both with temperature control. The reaction was set up with Mb at a concentration between 3 and 8 μM at 25 °C using either 50 mM phosphate, 50 mM Tris/HCl, or 50 mM acetate buffer system depending on the desired pH conditions (between the range of 3.92−8.0). Immediately after the first scan was completed, 100-fold excess of hydrogen peroxide (300−800 μM) was added to rapidly generate Cpd II. Two scans after the addition of hydrogen peroxide, a catalytic amount of catalase[12,15] (1 μL aliquot, resulting in ≤400 nM concentrations in the cuvette) was added in order to eliminate excess peroxide and prevent disruptive side reactions. The amount of catalase used had an activity of 530 μM s^{-1}, indicating that any excess peroxide used was consumed before the following scan upon catalase addition. The reaction was also probed using equimolar hydrogen peroxide concentrations with Mb concentrations of 3−8 μM at 25 °C and pH 5.5, 6.0, 6.5, and 7.0. The hydrogen peroxide was again added following the first scan; however, no catalase was used for the equimolar experiments. In both saturating and equimolar peroxide conditions, the Cary60 was set to record the absorbance every 2 nm from 700 to 300 nm at a scan rate of 9600 nm/min (resulting in a 6 s scan time) for 2 to 6 h depending on the pH conditions. HP8452A was set to record the absorbance from 700 to 300 nm every 2.6 s for 2 h or less for the faster reactions under lower-pH conditions.

2.3. Concentration-Dependent Reactions. In order to evaluate how the concentration of hydrogen peroxide affected the rate, the same reactions were run for Mb concentration 2−4 μM at 25 °C using a 50 mM acetate buffer system at pH 5.5. The reaction was run at hydrogen peroxide concentrations between 2 and 700 μM. The reaction was observed on an OLIS HP8452A diode array spectrophotometer. Under all reaction conditions above a single turnover (>4 μM), the catalytic amount of catalase was added during the fourth scan (∼10 s into the reaction) to remove the excess hydrogen peroxide before the Cpd II autoreduction proceeded to a measurable degree.

The Mb concentration-dependent runs were also observed on the OLIS HP8452A diode array spectrophotometer. The reaction conditions included varying the Mb concentration from ∼1 to ∼13 μM at 25 °C. The Mb concentration-dependent reactions were run in both a 50 mM phosphate buffer system at pH 6.8 and a 50 mM acetate buffer system at pH 5.0. The reaction was initiated after the first scan using the saturating 100-fold hydrogen peroxide concentration, followed by a catalytic amount of catalase to remove excess peroxide prior to appreciable Cpd II autoreduction.

2.4. Data Analysis: Global Fitting and Rate Determination. The absorbance data from time-resolved spectroscopy were retrieved from the Cary and arranged in an *XYZ* plot, using *X* as the wavelength, *Y* as the time, and *Z* as the absorbance. The data could then be used for time-dependent, single-wavelength, 2D kinetic analysis (not reported here), as well as time-resolved full spectra global analysis. OLIS GlobalWorks software was used for singular value decomposition (SVD) analysis[25] to determine the spectra of reacting species and the best kinetic rate mechanism fits. All abstract spectral and kinetic features indicated the presence of at least

https://doi.org/10.1021/acsomega.2c02798
ACS Omega 2022, 7, 22906−22914

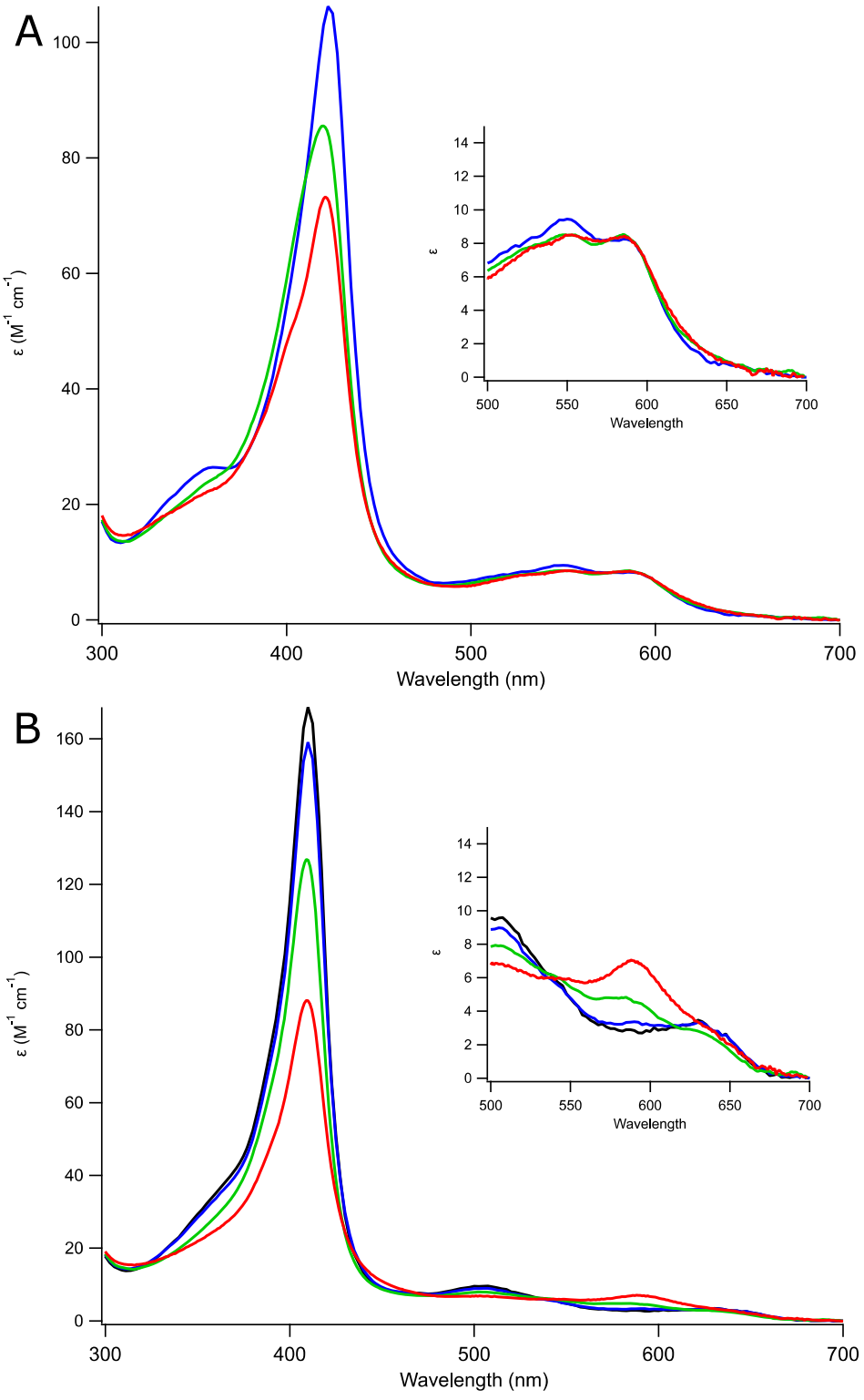

Figure 1. Normalized pH-dependent spectra of Mb treated with saturating peroxide. (A) Mb Cpd II spectra at pH 7.5 (blue, thick SVD), pH 5.5 (green thick SVD), and pH 3.92 (red thick SVD). Inset: The pH spectral features of the Q bands for Cpd II pH 7.5 (blue), pH 5.5 (green), and pH 3.92 (red). (B) Comparison of ferric Mb at pH 7.5 (black) to oxidatively damaged ferric Mb extrapolated from SVD analysis at pH 7.5 (blue), pH 5.5 (green), and pH 3.92 (red).

three meaningful factors. In order to evaluate the model for the three species, an irreversible sequential A → B → C model was used and a nominal Cpd II formation A → B, k_1, rate could be extracted. The conditions of this study were not optimum for accurate calculation of k_1, so it is not reported here, although it is qualitatively consistent with the previously published peroxide-dependent data.[6] The Cpd II autoreduction rate k_2 could be extracted from this analysis as well except for the slowest reactions (at pH > 7.0). For these conditions, the eigenvalue corresponding to initial ferric was underrepre-

https://doi.org/10.1021/acsomega.2c02798
ACS Omega 2022, 7, 22906−22914

sented, so the reaction data were fit starting at the 20 s time mark to an irreversible two-species B → C model. Both global analysis models do not require input parameters in the OLIS GlobalWorks software. This model was run for faster reactions at lower pH as well and gave k_2 values statistically identical to those using the three-species model.

3. RESULTS

3.1. pH-Dependent Spectra of Mb Cpd II. Using global analysis and saturating peroxide conditions, we are able to probe Cpd II spectra and kinetics under pH conditions below pH 5.0 without interferences otherwise seen at low pH. Under lower-pH conditions, the rate of formation, "k_1", of Cpd II is competitive with the autoreduction rate, k_2, of Cpd II autoreduction, thus making it difficult to fully resolve the Cpd II spectral features. Once the k_2 begins to become greater than k_1, Cpd II never builds up enough to accurately determine the rates and spectral features across the visible range for a global analysis program with the limitation of lacking initial spectral inputs. We consider this an inevitable limitation of analyses using single-turnover reaction conditions,[1] motivating our use of excess peroxide in the present study. Using saturating conditions reported in this article, the high-valent intermediate Cpd II quickly builds up to substantial percentages (>50% even at the lowest pH), allowing both global analysis programs and raw spectral data to show clear Cpd II spectra.

Mb oxidation with a saturating level of peroxide rapidly generated the spectra of Cpd II at all pH values (Figure 1A). These spectra had Soret maxima at 422 nm with Q band peaks at 550 and 585 nm as previously reported[6] for both sperm whale and horse heart Mb in stopped-flow rapid-scan studies by Egawa et al.[6,26] Figure 1A shows the computed spectrum for this species derived from SVD analyses of the datasets described in Section 2. Since the conversion to Cpd II is rapid and near-quantitative under saturating conditions, the fitted spectra closely resemble the early time-resolved absorption scans (17−30 s) indicating that they are not a fitting artifact.

Our Cpd II spectra display pH-dependent features both in the Q band and the Soret regions. The same absorption maxima are seen across the full pH range, but relative intensities vary with pH. The *Q* bands' maximal intensity is pH-sensitive, with the 550 nm one being less intense and almost equivalent in intensity to the 585 nm band at pHs ≤6.0 (Figure 1A inset, green, pH 5.5 and red, pH 3.92). Under pH conditions >6.0, the 550 nm peak is more intense than the 585 nm peak and the 585 nm only shows the smallest decrease in intensity as compared to lower-pH values. This trend is consistent with some but not all of the previous studies[2,4−6,24,27] that report pH-dependent spectroscopy differences. While there is a general agreement on the spectral features of the more stable Cpd II under neutral or basic conditions, other researchers describe different absorption band positions in their "acid form" spectra, including a relative Q band maximum around 529 nm and a near absence of significant absorption around 586 nm.[2,3,24] Their "acid form" Soret maximum was reported to shift slightly from 424 to 421 nm.[24] Our data in Figure 1A demonstrate a suggestion of a shoulder around 520 nm, and the 585 nm peak barely decreases at the lowest pH of 3.92, similar to what has been reported in low-temperature solution and crystals.[27] Our observed Soret lambda maximum occurs at the same wavelength (422 nm) at all pHs; however, the intensity of the absorption decreases with pH (Figure 1A). In order to evaluate the pH dependence of this decrease, we determined the Cpd II Soret maximum molar absorptivity under all pH conditions tested from pH 3.92 to pH 8.0 (Figure 2). The

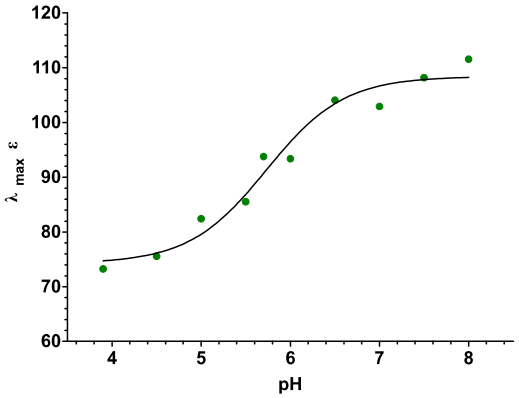

Figure 2. Graph of the molar absorptivity of Mb compound II at its Soret lambda max at 422 nm at all pHs from pH 3.92 to 8.0.

decreasing intensity of the lambda maximum has a sigmoidal appearance with an inflection point at a pH of 5.7 ± 0.1, suggesting that this is a pK_a marking the transition between reported[3,24] "acid" and "basic" forms of Cpd II. We consider this "acid form" not likely to be a protonated ferryl Cpd II as the inflection point indicates a pK_a substantially above pHs with spectroscopically observed deprotonated Cpd II.[4,5] Rather, the inflection point does indicate a pK_a similar to a reported[12] pK_a of the distal histidine of horse heart Mb.

The high-valent Mb ultimately decays via autoreduction pathways to form an oxidatively damaged ferric Mb, which can be seen in the SVD spectra (Figure 1B) and the raw data. As compared to Cpd II, the oxidatively damaged ferric Mb displays more qualitative differences between the spectra at low pH and that at high pH. At higher pHs, the oxidatively damaged Mb spectra closely resemble those of the unreacted ferric Mb. At the lower pHs, the oxidatively damaged Mb spectrum has a 30−50% relative reduction in Soret intensity compared to the initial ferric Mb (Figure 1B) and the Q band structure is altered from the original ferric Mb Q band features (Figure 1B inset). These features resemble those of a crosslinked porphyrin to protein product, as investigated in detail previously.[7,8,20]

Note that the lowest pH used for this study was 3.92 in acetate buffer due to the protein fold destabilizing under acidic conditions. In our study, this is indicated by a clear change in the Soret spectra of the unreacted ferric Mb (Figure S1, Supporting Information). In all citrate buffers, and under pH conditions less than 3.92 in acetate buffer, the ferric Soret lambda maximum decreases and a shoulder appears at 362 nm, while the Q bands lose a little intensity at 505 nm, but no change occurs at 632 nm. We attribute these features to fold destabilization on the initial Mb and for this report use only data that do not display a disruption in protein stability as evidenced by their initial ferric spectra. The compound II generated under these conditions shows a similar 362 nm shoulder on the Soret bands, a decrease in the 585 nm band Q band feature, and a significant increase in absorption near 505 nm (Figure S1). These Q band features are not seen in our Cpd II spectra of intact Mb at pH 3.92 and above (i.e., in the

https://doi.org/10.1021/acsomega.2c02798
ACS Omega 2022, 7, 22906−22914

absence of protein unfolding or destabilization), and we caution that they may indicate some destabilization in previously reported pH-dependent Cpd II forms using uncommon buffer systems[3,24] and pH jump techniques.[2]

3.2. Mb-Dependent Kinetics for the Autoreduction of Ferryl Mb to the Ferric State. During the inspection of kinetic data from the studies reported in Figure 2 and Section 3.4 below, we saw unexpected indications that the autoreduction kinetics varied somewhat with the initial Mb concentration. To investigate this possibility, we undertook a systematic study of autoreduction rate k_2 at two pH values above and below the pH 5.7 inflection point of Figure 2. As indicated in Section 2, the reaction conditions included varying the Mb concentration from ~1 to ~13 μM at 25 °C. The Mb concentration-dependent reactions were run in both a 50 mM phosphate buffer system at pH 6.8 and a 50 mM acetate buffer system at pH 5.0. In order to model k_2, the data up to 1500 s (pH 5.0) or 4000 s (pH 6.8) were fit using the three meaningful recovered eigen factors and an irreversible sequential A → B → C model. The OLIS program was able to generate rates and SVD spectra with consistent handles for each species at varying Mb concentrations at both pH 5.0 and pH 6.8 (above and below the transition pH of the Cpd II "acid and basic" forms determined in Figure 2).

The Cpd II autoreduction k_2 rates at pH 5.0 (Figure 3) and 6.8 (Figure 4) demonstrate differing patterns of Mb

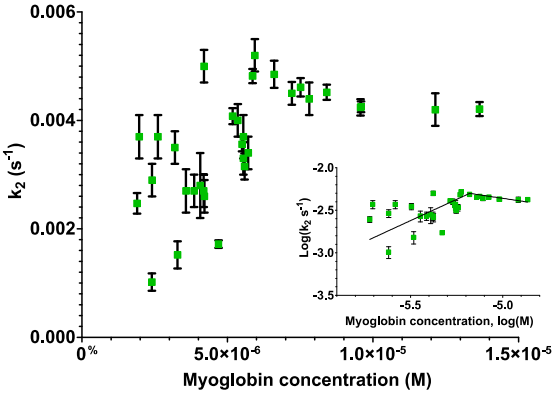

Figure 3. Observed rates (s^{-1}) for the autoreduction of Cpd II to oxidatively damaged ferric Mb vs Mb concentration in M at pH 5.0. Inset: the log of k_2 vs log of Mb concentration and the segmental linear fit of the data (solid line). Each kinetic rate data point reports the standard error of the SVD global analysis fit of the data run using error bars and where error bars are not visible, the error is smaller than the marker for that point.

concentration dependence; to illustrate this, the log of rate versus the log of concentration plots was fit to a segmental linear regression. At pH 5.0, where the "acid form" of Cpd II autoreduces, the rate appears to rise with concentration at a slope of 1.0 ± 0.2 until approximately 6.6 μM, where the rate levels off and becomes Mb-independent (Figure 3 inset). This suggests that the k_2 rate for the "acid form" of Cpd II may be dependent on a first-order Mb process up to ~6.6 μM, where the rate becomes zero-order for Mb. In contrast to the "acid form" Cpd II, at pH 6.8, the "basic form" Cpd II's autoreduction rate decreases with increasing concentration at a slope of −1.0 ± 0.1 up to the same 6.6 μM Mb concentration at which the rate once more levels off (Figure 4 inset). We are undertaking further study of these dependencies.

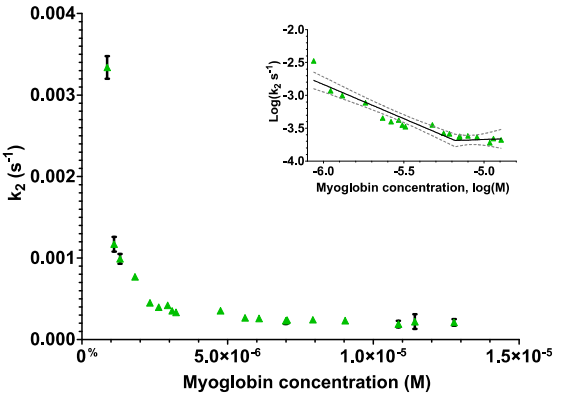

Figure 4. Observed rates (s^{-1}) for the autoreduction of Cpd II to oxidatively damaged ferric Mb vs Mb concentration in M at pH 6.8. Inset: the log of k_2 vs log of Mb concentration and the segmental linear fit of the data (black, solid line) with the confidence intervals of the fit (gray, dashed line). Each kinetic rate data point reports the standard error of the SVD global analysis fit of the data run using error bars, and where error bars are not visible, the error is smaller than the marker for that point.

3.3. Peroxide-Dependent Kinetics for the Autoreduction of Ferryl Mb to the Ferric State. To complement the Mb dependency studies, we conducted a similar investigation of the dependence of the autoreduction on the peroxide concentration used to initiate Cpd II formation. Whereas Cpd II formation is reliant on a bimolecular reaction with hydrogen peroxide (rate-limiting step "k_1") to form Cpd II, as previously observed in Mb,[6] we assumed no further peroxide effects on the reaction after the catalase removal of excess peroxide at early times in the observation (<20 s). In order to determine any peroxide dependency in "k_2", the Cpd II autoreduction rate to an oxidatively damaged ferric Mb, the peroxide concentration was varied at pH 5.5, the lowest pH for which Cpd II is clearly observed to build up at low (equimolar) hydrogen peroxide concentrations. Under reaction conditions with excess peroxide concentrations, catalase was added following the buildup of Cpd II.

As in the other experiments, the peroxide-dependent data were fit using global analysis. The entire time set of the data, from 0 s to ~3500 s, was modeled for three species using an irreversible sequential A → B → C model. For all of the peroxide-dependent data, abstract spectral and kinetic features still indicated the presence of at least three meaningful factors. The resulting Cpd II autoreduction B → C, k_2, observed rate was reported as a rate k_{2obs} (s^{-1}) and graphed versus hydrogen peroxide concentration in Figure 5.

The log of rate versus the log of peroxide concentration plots (insets of Figure 5) indicates that certain concentration ranges of peroxide concentrations show enhanced rates for the subsequent Cpd II autoreduction. The k_{2obs} rate (Figure 5) appears to increase with peroxide concentration roughly linearly before leveling off to a higher rate from around 10-fold (around 30 μM) until ~40-fold (around 130 μM). Then, the rate decreases with a peroxide concentration up to about 250 μM, above which it is stable at roughly 1×10^{-3} s^{-1}. The observed rate above 250 μM, which represents the range of peroxide concentrations used during all of the remainders of our data, also is roughly the same as the rate constant obtained at this pH in single-turnover experiments. While this region of enhanced k_{2obs} rate may suggest a reactivity difference for the

https://doi.org/10.1021/acsomega.2c02798
ACS Omega 2022, 7, 22906−22914

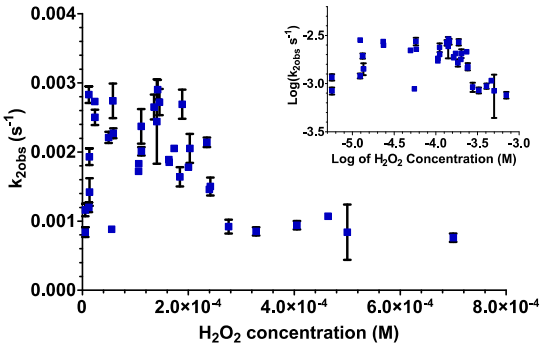

Figure 5. Observed rates (s^{-1}) for the autoreduction of Cpd II to oxidatively damaged ferric Mb, k_2, vs hydrogen peroxide (H_2O_2) concentration in M at pH 5.5. Inset: the log of k_{2obs} vs log of H_2O_2 concentration. Each kinetic rate data point reports the standard error of the SVD global analysis fit of the data run using error bars, and where error bars are not visible, the error is smaller than the marker for that point.

Cpd II formed under these reaction conditions, we cannot currently hypothesize further possible explanations for this effect.

3.4. pH-Dependent Kinetics for the Autoreduction of Ferryl Mb to the Ferric State under Saturating Peroxide Conditions. In order to assess the pH-dependent kinetics of high-valent Cpd II decay in the autoreduction mechanism, SVD analyses were performed for the time-resolved spectral data at concentrations in the Mb-dependent region at pH from 3.92 to 8.0. In order to model the rate of ferric to Cpd II, data at pH higher than 5.5 were modeled in two timescales: an early ~200 s to model the ferric to Cpd II conversion and a later timescale starting at the point where Cpd II is the dominant species. In this paper, we focus on Cpd II autoreduction for all stable pH conditions of horse heart Mb. SVD spectra fit under all three pH conditions are shown in Figure 6, with the corresponding kinetic fits and residuals in Figure 7. The k_2 rates (B → C) were consistent within error when comparing both models to each other at all pHs where modeling from time zero was possible and produced a pH-dependent rate (Figure 8).

When the observed rate is plotted versus pH, the decay has no observed inflection point, indicating a $pK_a < 3.9 \pm 0.2$ (Figure 8). This data can also be transformed to fit a log (rate) versus the pH plot to assess the proton dependence on the rate (inset Figure 8). When our data in the Mb concentration-dependent region is graphed in a log (rate) versus pH plot, the corresponding slope is −0.48 ± 0.04, which indicates that the reaction is dependent on essentially "half a proton" over the pH 4−8 range. This unexpected finding differs from the single-turnover data by Reeder and Wilson[1] over an overlapping pH range. As seen in Figure 9, our results and those of Reeder and Wilson[1] clearly lie on distinct lines which intersect near pH 6. To verify that the differing proton dependence is not the result of the different initial peroxide concentrations, we also include data we previously obtained at 3−5 μM Mb using single-turnover peroxide conditions (pH 5.5, 6.0, 6.5, and 7.0). We note that these fall on the same line as our data (solid line) collected with saturating peroxide conditions. Possible explanations are discussed below.

4. DISCUSSION

As described above, using global analysis and saturating peroxide conditions allows this study to probe Cpd II spectra and kinetics under pH conditions below pH 5.0 without interferences otherwise seen at low pH. By carefully using spectral characterization to verify that unreacted ferric Mb is stable and folded, we were able to perform direct oxidation to Cpd II with pH conditions up to 3.9, a full pH unit lower than that previously reported.[1] We consider the added spectral and kinetic data for pH < 5 a major contribution of the present study. The uncovered pH dependency of the molar intensity to the Soret's 422 nm lambda maximum (Figure 2) described in this article is of interest as it has not been described or isolated previously. This pH dependence suggests that a protonation event in the proximity of the heme disturbs the electronics of the system while not reducing the high-valent species.

Originally, this protonation event was assumed to be on the ferryl oxo and generates a species referred to as the "base form" and "acid form" of Cpd II[2,24] assigned respectively as ferryl (Fe^{IV}=O) and ferryl hydroxide (Fe^{IV}−OH) by several groups. However, when examining the pH profile of Cpd II, we consider that this protonation event is instead likely to be related to a hydrogen bonding event at an acid site near the Fe^{IV}=O moiety. The proximal His in Mb is a potential protonation site; however, as indicated by calculated proton affinities,[2] the pK_a of the proximal His is closer to the pK_a of ferric hydroxide and Mb Cpd 0, which is in the range of 8−10. The distal His64 is also another polar ionizable group in the

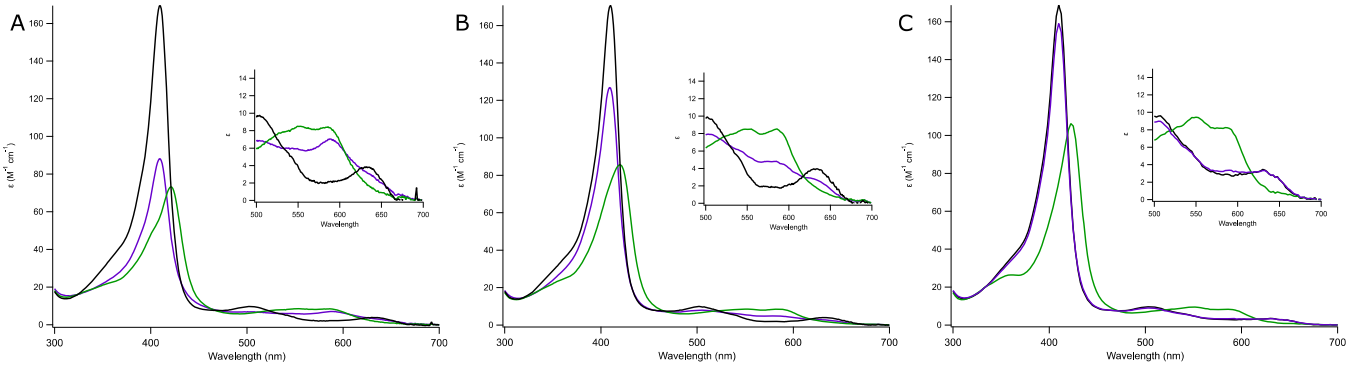

Figure 6. Spectral decomposition (SD) spectra from global analysis fits of Mb reaction with saturating hydrogen peroxide graphed as molar absorptivity based on the concentration of Mb vs wavelength. (A) SD spectra for ferric (black), Cpd II (green), and ferric oxidized (purple) at pH 3.92. Inset: Q band spectra. (B) SD spectra for ferric (black), Cpd II (green), and ferric oxidized (purple) at pH 5.5. (C) SD spectra for ferric (black), Cpd II (green), and ferric oxidized (purple) at pH 7.5.

https://doi.org/10.1021/acsomega.2c02798
ACS Omega 2022, 7, 22906−22914

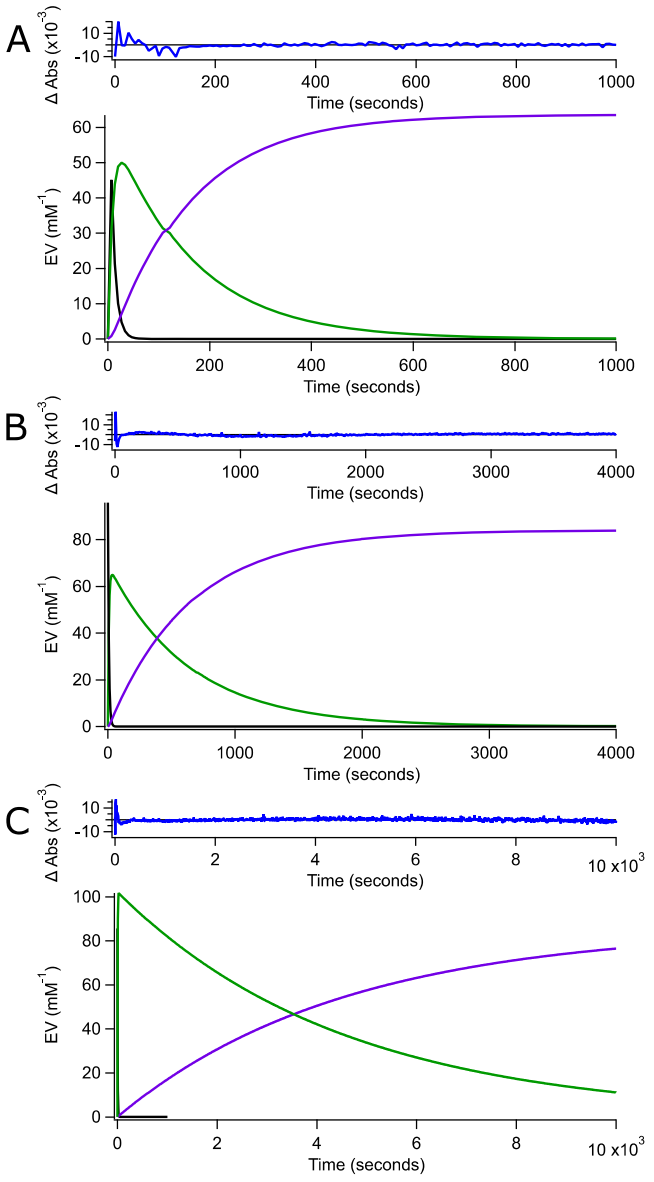

Figure 7. SVD analysis produced species decay and overall residual fits. Upper graphs are overall residuals of the SVD fit using a three species (A → B → C) model graphed as a change in absorbance vs time (blue). Lower graphs show the change in species over time by graphing relative percentage vs time (ferric is black, Cpd II is green, and ferric oxidized is purple). SVD analysis performed for reactions at (A) pH 3.92, (B) pH 5.5, and (C) pH 7.5.

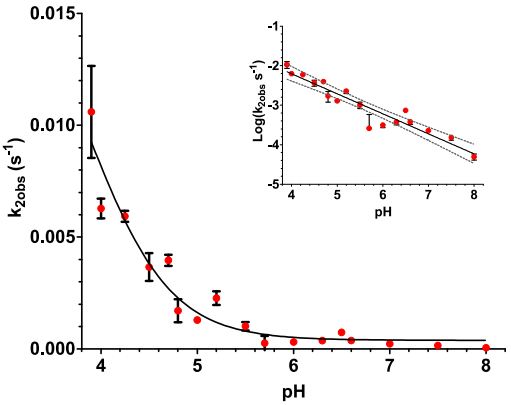

Figure 8. Average observed rates (s^{-1}) for the autoreduction of Cpd II to oxidatively damaged ferric Mb vs pH values. Inset: the log of k_2 vs pH (log of H^+ concentration) and the linear fit of the data (solid line) with the confidence intervals of the fit (dashed line). Each kinetic rate reports the standard error of the fits for the data at each pH using error bars, and where error bars are not visible, the error is smaller than the marker for that point.

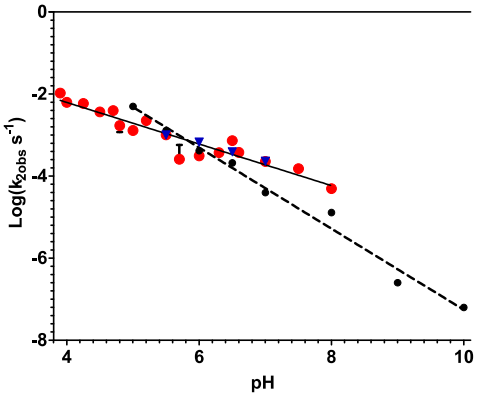

Figure 9. Log of average observed rates (s^{-1}) for the autoreduction of Cpd II to oxidatively damaged ferric Mb vs pH values. The red circles are data determined in this article, and the solid black line is the linear fit of our data. The black dots are the published single-turnover data of Reeder and Wilson,[1] and the dashed line is the linear fit for their data. The blue triangles are our results at ~3 μM Mb using single-turnover conditions.

vicinity, and we consider that the pH-dependent Cpd II is likely due to the formation of a stable or low barrier hydrogen bond between a protonated His64 Nε and the ferryl oxo. Fitting the molar absorptivity of the Soret at 422 nm to a sigmoidal dependency provides a pK_a of ~5.7 ± 0.1 (Figure 2), which is close to values reported for the pK_a of the distal His in several different Mb species[28−30] and an exact match to the Ru-modified horse heart.[12] Thus, we consider the most likely site of the protonation to be the His64 Nε, providing Cpd II with a hydrogen bonding group for pHs near and below 5.7 ± 0.1. Protonation at His64 Nε would also support a hydrogen bonding event with the ferryl oxo as the likely cause of the electronic change observable in visible[27] (this article), Raman,[4,5] and Mossbauer spectroscopy[5] while remaining unchanged in Fe EXAFS.[5] One notable finding is that while we observe indications of a spectral transition attributable to a pK_a consistent with that of protonation of the distal His64, we do not reproduce the kinetic transition <pH 5 of refs1 and[2] that was interpreted as the hypothesized protonated ferryl[1,2] species; instead, our kinetic data produces a kinetic transition <3.9 ± 0.2, supporting rather the interpretations of Green and co-workers.[4,5]

Thus, our kinetic data indicate that the protonation of the ferryl oxo of Cpd II is still considered part of the rate-limiting portion of the reaction. This is evident at low Mb concentrations as the mechanism is still influenced by pH with no inflection point even when the pH is as low as 3.9 (Figure 8) and has a constant slope without a breakpoint in the stable pH range 3.9−8, which we probe here in this article. This data implies that the proton that limits the rate has a pK_a of below pH 3.9, which is similar to the previously reported experimentally determined pK_a of Cpd II in His-ligated horseradish peroxidase[31] and the spectroscopic data of Mb Cpd II which displays no protonation of Cpd II.[5] Each of the previously published experiments is explored at a very high Mb

https://doi.org/10.1021/acsomega.2c02798
ACS Omega 2022, 7, 22906−22914

concentration, as were the Ru-modified Mb experiments,[12,13] which demonstrated that the reaction was limited not on reorganization energy or electron transfer but rather the proton transfer event. However, our data uncover additional features that impact the kinetics, including that this rate-limiting protonation is not dependent on a single proton[1] but rather a half a proton.

As depicted in Figure 9, it is not easy to reconcile the results of our kinetic data with previously published single-turnover UV−visible data.[1] While we were able to probe the important pH range from 3.9 to 5 and investigated the higher pH region above pH 8, there is a large pH overlap in the kinetic data sets. While the observed rates between pH 5 and 8 are within comparable orders of magnitude, the trend lines are clearly distinct and each adheres to the computed reaction order (1^1 and 0.48 ± 0.04; this article) within the experimental error. We consider our SVD full spectral analysis a preferable analysis method, especially since the likely combination of oxidized ferric products may have small pH-dependent differences of absorption at both the Soret region wavelengths chosen for their fit and in the Q band region included in our methodology. Nevertheless, their data demonstrate fairly clean first-order decay at the longer observation times, and they quote respectable R^2 values for their fits. Since our single-turnover data lie on our trendline rather than that of theirs in Figure 4,[1] we do not believe that our saturated peroxide conditions, presence of catalase, or peroxide dependency in general are the cause of the distinction. We do acknowledge that our rates may be impacted by our measured Mb dependency for k_2, as most of our data were obtained with Mb concentrations in the 3−5 μM range, where we see a variation of k_2 as compared to the value at 10 μM used in their study.[1]

The half-order proton dependency for the Cpd II autoreduction rate is an unusual feature of our data. This, along with the unexpected autoreduction rate dependence on Mb and initial peroxide concentration, is a clear indication of a more complex reaction mechanism for the Cpd II decay than originally assumed. Fractional order in rate laws generally indicates that the particular mechanistic step being examined is a series of steps rather than one isolated step. Half-order rates have been isolated before in many radical initiation/propagation mechanisms, from peroxides to metal complex oxidations.[32−34] Thus, we are proposing that in the Mb Cpd II autoreduction, a radical propagation mechanism may be favored or occurs with a larger proportion, at least at low Mb concentrations. Kinetic isotope effect studies and further studies to explore how different reaction oxidation sites affect mechanistic kinetics are currently being investigated.

■ ASSOCIATED CONTENT

Supporting Information

The Supporting Information is available free of charge at https://pubs.acs.org/doi/10.1021/acsomega.2c02798.

Graph of ferric Mb in acetate buffer systems at both stable and unstable pHs (PDF)

■ AUTHOR INFORMATION

Corresponding Author

Heather R. Williamson − *Department of Chemistry, Xavier University of Louisiana, New Orleans, Louisiana 70125, United States;* orcid.org/0000-0002-2413-659X; Email: hwillia8@xula.edu

Authors

Kamisha R. Hill − *Department of Chemistry, Xavier University of Louisiana, New Orleans, Louisiana 70125, United States;* Present Address: Department of Chemistry and Biochemistry, Georgia Institute of Technology, North Ave NW, Atlanta, GA, 30332; orcid.org/0000-0003-1575-3382

Breanna G. Bailey − *Department of Chemistry, Xavier University of Louisiana, New Orleans, Louisiana 70125, United States*

Meghan B. Mouton − *Department of Chemistry, Xavier University of Louisiana, New Orleans, Louisiana 70125, United States*

Complete contact information is available at: https://pubs.acs.org/10.1021/acsomega.2c02798

Notes

The authors declare no competing financial interest.

UniProt ID: A0A452GEN9—*Equus caballus* (Horse) Myoglobin.

■ ACKNOWLEDGMENTS

This work was partially supported by the National Institute of Health NIGMS-BUILD grant numbers 2RL5GM118966, 5UL1GM118967, and TL4GM118968 and by the National Institute of Health under the award number SC2GM136557. This publication also was made possible by support from the Louisiana Cancer Research Consortium (LCRC) and the RCMI grant number 5G12MD007595 from the National Institute on Minority Health and Health Disparities. The content is solely the responsibility of the authors and does not necessarily represent the official views of the NIH, LCRC, or RCMI. We also would like to thank Zajae Lee, Hassan Niang, and Kanhiya Dickenson for their help in preparing Mb samples.

■ ABBREVIATIONS

UV, ultraviolet
Mb, myoglobin
SVD, singular value decomposition
Cpd I, compound I, high-valent ferryl heme with a porphyrin radical cation
Cpd II, compound II, a high-valent ferryl heme
MCD, magnetic circular dichroism
RR, resonance Raman
EXAFS, extended X-ray absorption fine structure
2D, two-dimensional
SM, supplemental material
His, histidine, an amino acid residue
ET, electron transfer
PT/ET, proton transfer followed by electron transfer
PCET, proton-coupled electron transfer (concerted proton and electron transfer)

■ REFERENCES

(1) Reeder, B. J.; Wilson, M. T. The Effects of PH on the Mechanism of Hydrogen Peroxide and Lipid Hydroperoxide Consumption by Myoglobin: A Role for the Protonated Ferryl Species. *Free Radical Biol. Med.* **2001**, *30*, 1311−1318.

(2) Silaghi-Dumitrescu, R.; Reeder, B. J.; Nicholls, P.; Cooper, C. E.; Wilson, M. T. Ferryl Haem Protonation Gates Peroxidatic Reactivity in Globins. *Biochem. J.* **2007**, *403*, 391−395.
(3) Foote, N.; Gadsby, P. M. A.; Greenwood, C.; Thomson, A. J. PH-Dependent Forms of the Ferryl Haem in Myoglobin Peroxide Analysed by Variable-Temperature Magnetic Circular Dichroism. *Biochem. J.* **1989**, *261*, 515−522.
(4) Behan, R. K.; Green, M. T. On the Status of Ferryl Protonation. *J. Inorg. Biochem.* **2006**, *100*, 448−459.
(5) Yosca, T. H.; Behan, R. K.; Krest, C. M.; Onderko, E. L.; Langston, M. C.; Green, M. T. Setting an Upper Limit on the Myoglobin Iron(IV)Hydroxide p K a : Insight into Axial Ligand Tuning in Heme Protein Catalysis. *J. Am. Chem. Soc.* **2014**, *136*, 9124−9131.
(6) Egawa, T.; Shimada, H.; Ishimura, Y. Formation of Compound I in the Reaction of Native Myoglobins with Hydrogen Peroxide. *J. Biol. Chem.* **2000**, *275*, 34858−34866.
(7) Reeder, B. J.; Svistunenko, D. A.; Sharpe, M. A.; Wilson, M. T. Characteristics and Mechanism of Formation of Peroxide-Induced Heme to Protein Cross-Linking in Myoglobin. *Biochemistry* **2002**, *41*, 367−375.
(8) Catalano, C. E.; Choe, Y. S.; Ortiz de Montellano, P. R. Reactions of the Protein Radical in Peroxide-Treated Myoglobin. *J. Biol. Chem.* **1989**, *264*, 10534−10541.
(9) Reeder, B. J.; Cutruzzola, F.; Bigotti, M. G.; Hider, R. C.; Wilson, M. T. Tyrosine as a Redox-Active Center in Electron Transfer to Ferryl Heme in Globins. *Free Radical Biol. Med.* **2008**, *44*, 274−283.
(10) Davies, M. J. Identification of a Globin Free Radical in Equine Myoglobin Treated with Peroxides. *Biochim. Biophys. Acta, Protein Struct. Mol. Enzymol.* **1991**, *1077*, 86−90.
(11) Irwin, J. A.; Østdal, H.; Davies, M. J. Myoglobin-Induced Oxidative Damage: Evidence for Radical Transfer from Oxidized Myoglobin to Other Proteins and Antioxidants. *Arch. Biochem. Biophys.* **1999**, *362*, 94−104.
(12) Fenwick, C. W.; English, A. M.; Wishart, J. F. PH and Driving Force Dependence of Intramolecular Oxyferryl Heme Reduction in Myoglobin. *J. Am. Chem. Soc.* **1997**, *119*, 4758−4764.
(13) Fenwick, C.; Marmor, S.; Govindaraju, K.; English, A. M.; Wishart, J. F.; Sun, J. Rate of Intramolecular Reduction of Oxyferryl Iron in Horse Heart Myoglobin. *J. Am. Chem. Soc.* **1994**, *116*, 3169−3170.
(14) Davydov, R.; Osborne, R. L.; Kim, S. H.; Dawson, J. H.; Hoffman, B. M. EPR and ENDOR Studies of Cryoreduced Compounds II of Peroxidases and Myoglobin. Proton-Coupled Electron Transfer and Protonation Status of Ferryl Hemes. *Biochemistry* **2008**, *47*, 5147−5155.
(15) Fenwick, C. W.; English, A. M. Trapping and LC−MS Identification of Protein Radicals Formed in the Horse Heart Metmyoglobin−H $_2$ O $_2$ Reaction. *J. Am. Chem. Soc.* **1996**, *118*, 12236−12237.
(16) Lardinois, O. M.; Ortiz de Montellano, P. R. Autoreduction of Ferryl Myoglobin: Discrimination among the Three Tyrosine and Two Tryptophan Residues as Electron Donors. *Biochemistry* **2004**, *43*, 4601−4610.
(17) Mannino, M. H.; Patel, R. S.; Eccardt, A. M.; Janowiak, B. E.; Wood, D. C.; He, F.; Fisher, J. S. Reversible Oxidative Modifications in Myoglobin and Functional Implications. *Antioxidants* **2020**, *9*, 549.
(18) Reeder, B. J.; Cutruzzola, F.; Bigotti, M. G.; Hider, R. C.; Wilson, M. T. Tyrosine as a Redox-Active Center in Electron Transfer to Ferryl Heme in Globins. *Free Radical Biol. Med.* **2008**, *44*, 274−283.
(19) Detweiler, C. D.; Lardinois, O. M.; Deterding, L. J.; Ortiz de Montellano, P. R.; Tomer, K. B.; Mason, R. P. Identification of the Myoglobin Tyrosyl Radical by Immuno-Spin Trapping and Its Dimerization. *Free Radical Biol. Med.* **2005**, *38*, 969−976.
(20) Reeder, B. J.; Cutruzzolà, F.; Bigotti, M. G.; Watmough, N. J.; Wilson, M. T. Histidine and Not Tyrosine Is Required for the Peroxide-Induced Formation of Haem to Protein Cross-Linked Myoglobin. *IUBMB Life* **2007**, *59*, 477−489.
(21) Gunther, M. R. Probing the Free Radicals Formed in the Metmyoglobin−Hydrogen Peroxide Reaction. *Free Radical Biol. Med.* **2004**, *36*, 1345−1354.
(22) DeGray, J. A.; Gunther, M. R.; Tschirret-Guth, R.; de Montellano, P. R. O.; Mason, R. P. Peroxidation of a Specific Tryptophan of Metmyoglobin by Hydrogen Peroxide. *J. Biol. Chem.* **1997**, *272*, 2359−2362.
(23) Gunther, M. R.; Tschirret-Guth, R. A.; Lardinois, O. M.; Ortiz de Montellano, P. R. Tryptophan-14 Is the Preferred Site of DBNBS Spin Trapping in the Self-Peroxidation Reaction of Sperm Whale Metmyoglobin with a Single Equivalent of Hydrogen Peroxide. *Chem. Res. Toxicol.* **2003**, *16*, 652−660.
(24) Wittenberg, J. B. Acid and Alkaline Forms of the Higher Oxidation State of Kangaroo, Horse, and Sperm Whale Myoglobin. *J. Biol. Chem.* **1978**, *253*, 5694−5695.
(25) Rittle, J.; Younker, J. M.; Green, M. T. Cytochrome P450: The Active Oxidant and Its Spectrum. *Inorg. Chem.* **2010**, *49*, 3610−3617.
(26) Egawa, T.; Yoshioka, S.; Takahashi, S.; Hori, H.; Nagano, S.; Shimada, H.; Ishimori, K.; Morishima, I.; Suematsu, M.; Ishimura, Y. Kinetic and Spectroscopic Characterization of a Hydroperoxy Compound in the Reaction of Native Myoglobin with Hydrogen Peroxide. *J. Biol. Chem.* **2003**, *278*, 41597−41606.
(27) Hersleth, H.-P.; Ryde, U.; Rydberg, P.; Görbitz, C. H.; Andersson, K. K. Structures of the High-Valent Metal-Ion Haem-Oxygen Intermediates in Peroxidases, Oxygenases and Catalases. *J. Inorg. Biochem.* **2006**, *100*, 460−476.
(28) Cerda, J. F.; Roeder, M. H.; Houchins, D. N.; Guzman, C. X.; Amendola, E. J.; Castorino, J. D.; Fritz, A. L. Electrochemical Determination of Heme-Linked PKa Values and the Importance of Using Fluoride Binding in Heme Proteins. *Anal. Biochem.* **2013**, *443*, 75−77.
(29) Bashford, D.; Case, D. A.; Dalvit, C.; Tennant, L.; Wright, P. E. Electrostatic Calculations of Side-Chain PKa Values in Myoglobin and Comparison with NMR Data for Histidines. *Biochemistry* **1993**, *32*, 8045−8056.
(30) Asher, S. A.; Adams, M. L.; Schuster, T. M. Resonance Raman and Absorption Spectroscopic Detection of Distal Histidine-Fluoride Interactions in Human Methemoglobin Fluoride and Sperm Whale Metmyoglobin Fluoride: Measurements of Distal Histidine Ionization Constants. *Biochemistry* **1981**, *20*, 3339−3346.
(31) Sitter, A. J.; Reczek, C. M.; Terner, J. Heme-Linked Ionization of Horseradish Peroxidase Compound II Monitored by the Resonance Raman Fe(IV)=O Stretching Vibration. *J. Biol. Chem.* **1985**, *260*, 7515−7522.
(32) Look, J. L.; Wick, D. D.; Mayer, J. M.; Goldberg, K. I. Autoxidation of Platinum(IV) Hydrocarbyl Hydride Complexes To Form Platinum(IV) Hydrocarbyl Hydroperoxide Complexes. *Inorg. Chem.* **2009**, *48*, 1356−1369.
(33) Brandt, C.; van Eldik, R. Transition Metal-Catalyzed Oxidation of Sulfur(IV) Oxides. Atmospheric-Relevant Processes and Mechanisms. *Chem. Rev.* **1995**, *95*, 119−190.
(34) Zhang, W.; Singh, P.; Muir, D. Oxidative Precipitation of Manganese with SO2/O2 and Separation from Cobalt and Nickel. *Hydrometallurgy* **2002**, *63*, 127−135.

https://doi.org/10.1021/acsomega.2c02798
ACS Omega 2022, 7, 22906−22914